Supporting Information for

One-pot Synthesis of Size- and Morphology- Controlled 1-D Iron Oxide Nanochains with Manipulated Magnetic Properties

Qingliang He,[a,b] Tingting Yuan,[a] Xingru Yan,[a,b] Zhiping Luo,[c]

Neel Haldolaarachchige,[d] David P. Young,[d] Suying Wei,*[a,b] and Zhanhu Guo,*[a]

[a] *Integrated Composites Laboratory (ICL), Dan F. Smith Department of Chemical Engineering, Lamar University, Beaumont, Texas 77710 United States Tel: +1 409 880 7654 E-mail: zhanhu.guo@lamar.edu*

[b] *Department of Chemistry and Biochemistry, Lamar University, Beaumont, Texas 77710 United States Tel: +1 409 880 7976 E-mail: suying.wei@lamar.edu*

[c] *Department of Chemistry and Physics, Fayetteville State University, Fayetteville, NC 28301, United States*

[d] *Department of Physics and Astronomy, Louisiana State University, Baton Rouge, Louisiana 70803, United States*

Contents

1. Experimental

1.1. Materials

PP- MA (supplied by Baker Hughes Inc.) with two different molecular weights (chemical structures were shown in Scheme S2) were used: they are both homo-polypropylene with one terminal MA group attached through Alder-ENE reaction; the average numerical molecular weights (M_n) are ~ 2500 and 8000 g/mole. Iron(0) pentacarbonyl ($Fe(CO)_5$, 99%) was commercially obtained from Sigma Aldrich. Solvent xylene (laboratory grade, ρ=0.87 g/cm^3) was purchased from Fisher Scientific. All the chemicals were used as-received without any further treatment.

1.2. Synthesis of γ-Fe_2O_3 nanochains

The typical synthesis procedures of γ-Fe_2O_3 nanochains were demonstrated as below. Briefly, solid PP-MA (0.25 g, M_n≈8000 or M_n≈2500) was first added into 100 mL xylene in a three-neck flask and heated to reflux (140 °C) till the formation of a transparent solution, indicating a complete dissolution of PP-MA (~ 30 min). Second, brown $Fe(CO)_5$ (3.50 g) was injected into the hot mixed solution (solution became yellow). Then, the solution was further refluxed for 3 hours at 140 °C constantly to form a black colloid. After cooling, the final colloidal solution was poured to a large glass container to evaporate xylene in the fume hood. Then the black powders were dried in vacuum at room temperature oven for 24 hrs to form the final nanocomposites. For the synthesis of the transition intermediate consisting of flower shape γ-Fe_2O_3 nanoparticles and nanochains stabilized by PP-MA (M_n≈8000), 0.50 g PP-MA (M_n≈8000) was used according to the same aforementioned reaction conditions. For the synthesis of mono-dispersed core-shell nanoparticles, 0.5 PP-MA (M_n≈2500) was used according to the same aforementioned reaction conditions.

For the nanoparticles synthesized in Scheme S2, the same reaction conditions were used: different PP-grafted maleic anhydride (0.25 g) was first added in 100 mL xylene in a three-neck flask and heated to reflux (140 °C) till the formation of a transparent solution. Second, brown $Fe(CO)_5$ (3.5 g) was injected into the hot mixed solution (solution became yellow). Then, the solution was further refluxed for 3 hours at 140 °C constantly to form a black colloid. Finally, the colloids are used to prepare for the TEM samples.

1.3. Characterization

The morphologies of the as prepared Fe_2O_3 nanoparticles were observed by transmission electron microscopy (TEM) in a FEI TECNAI G2 F20 microscope at a working voltage of 200 kV. The samples were prepared from the hot colloidal solution by the end of synthesis process. One droplet of diluted solution containing the nanoparticles was dropped on a 400-mesh carbon coated copper grid (Electron Microscopy Sciences). The Selected area electron diffraction (SAED) patterns were taken using a large selected-area aperture and recorded using a Gatan SC1000 ORIUS CCD camera. In case the center beam is strong, a needle was placed in the center to block the beam for half of the exposure time (2 seconds). And then it was immediately removed away from the view area, so that the needle appeared in the pattern which blocked the center strong beam for half of the total exposure time.

For micro-structural evaluation in the scanning electron microscope (SEM), samples were mounted on an aluminum stub by using carbon tape. Then, samples were sputtered in a Hummer 6.2 system (15 mA AC for 30 sec), creating approximately a 1 nm thick film of Au. SEM used was a JEOL JSM 6700R in high vacuum mode.

For the magnetic measurements, a plastic drinking straw was utilized as the sample holder. A small portion of each specimen, ~5-10 mg, was loaded in the straw. The magnetic moment of the sample was measured in a commercial magnetometer (Quantum Design PPMS system) at room temperature, which is a Faraday-extraction type magnetometer. At each field value, 10 scans were measured and averaged.

Thermal stability was investigated using thermogravimetric analysis (TGA, TA Instruments Q-500). Samples were heated from room temperature to 700 °C at a constant heating rate of 20 °C/min under nitrogen gas atmosphere. The flow rate was 60 mL/min.

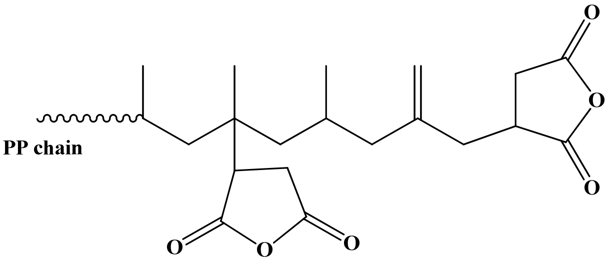

Scheme S1. Chemical structure of PP-g-MA ($M_n \approx 8000$g/mol).[1]

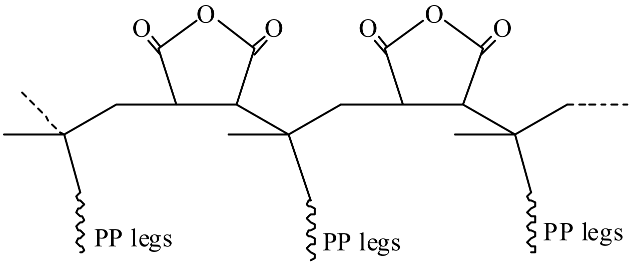

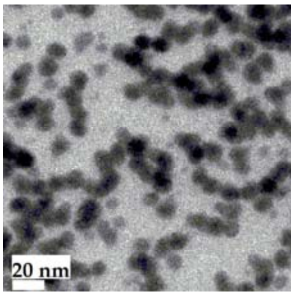

(a). Alternating maleic polypropylene homopolymer (with Mn ~ 2500 polypropylene "legs")

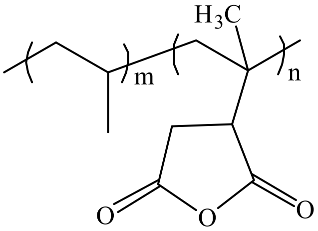

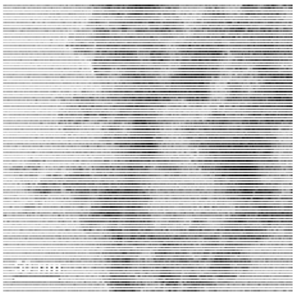

(b).Polypropylene-graft-maleic anhydride, average Mn ~3900

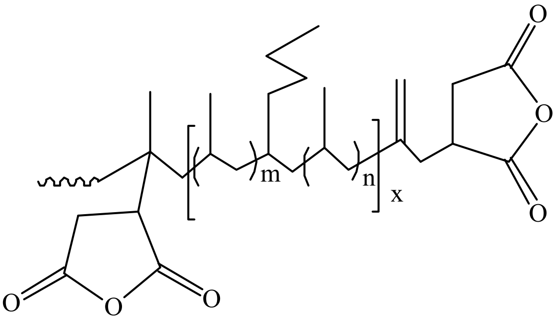

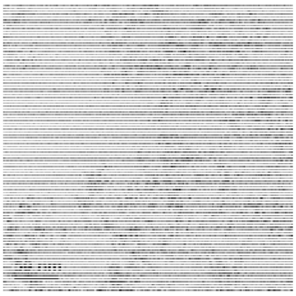

(c). Propylene-hexene copolymer with one maleic anhydride at one terminal and the other maleic anhydride grafted on the main chain, average Mn ~800

Scheme S2. Chemical structure of different PP-g-MA.

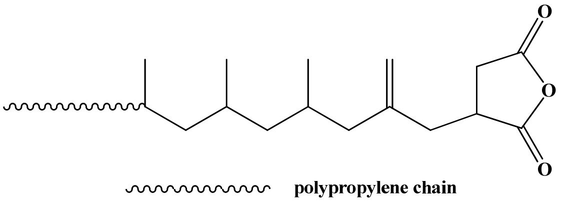

Scheme S3. Chemical structure of PP-MA with different molecular weights (~ 8000 and 2500 g/mol).

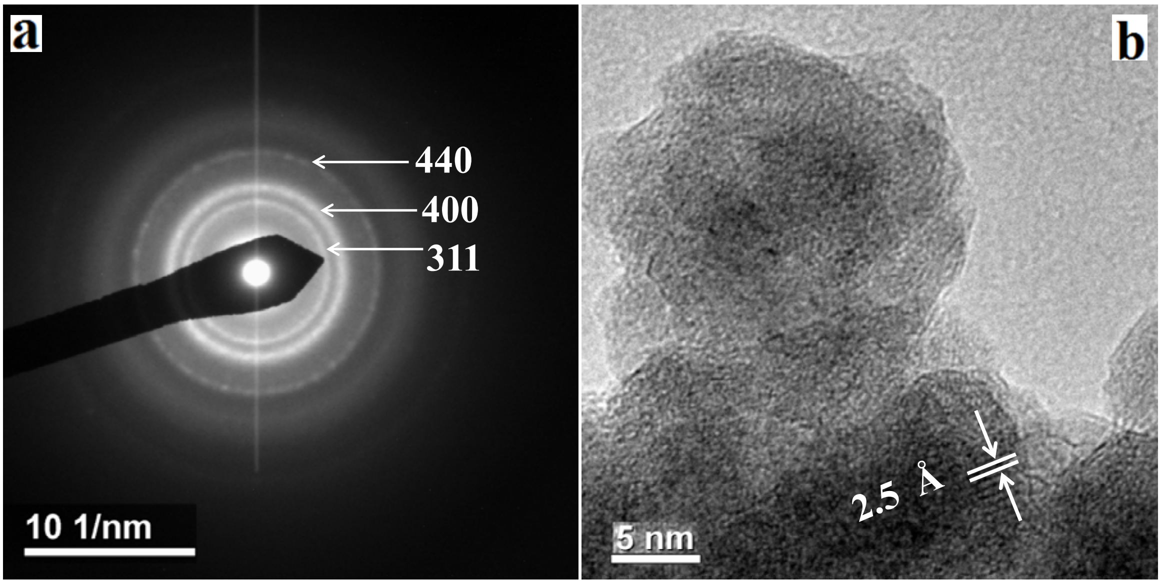

Fig. S1 a). SAED patterns and b). HRTEM lattice spacing of γ-Fe_2O_3 nanochains stabilized by PP-MA (Mn≈8000). The strong ring patterns in Fig. S1a are corresponding to (311), (400) and (440) planes of γ- Fe_2O_3 (PDF#39-1346). In Fig. S1b, the measured 2.5 Å lattice spacing can be assigned to the (311) plane of γ- Fe_2O_3 (PDF#39-1346). Reaction composition: 3.5 g $Fe(CO)_5$ in 100 mL xylene with 0.25 g PP-MA (Mn≈8000).

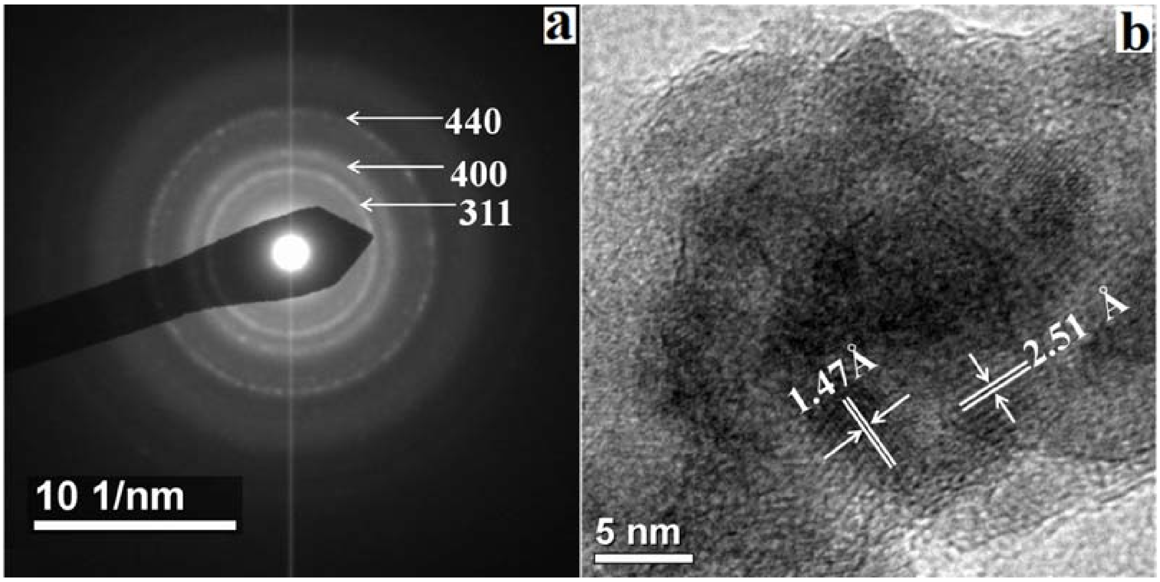

Fig. S2 a). SAED patterns and b). HRTEM lattice spacing of γ-Fe_2O_3 nanochains stabilized by PP-MA (M_n≈2500). In Fig. S2a, the strong ring patterns are corresponding to (311), (400), and (440) planes of γ- Fe_2O_3 (PDF#39-1346). Meanwhile, the measured 2.51 and 1.47 Å lattice spacing (Fig. S2b) are corresponding to the (311) and (440) planes of γ-Fe_2O_3 (PDF#39-1346). Reaction composition: 3.5 g $Fe(CO)_5$ in 100 mL xylene with 0.25 g PP-MA(M_n≈2500).

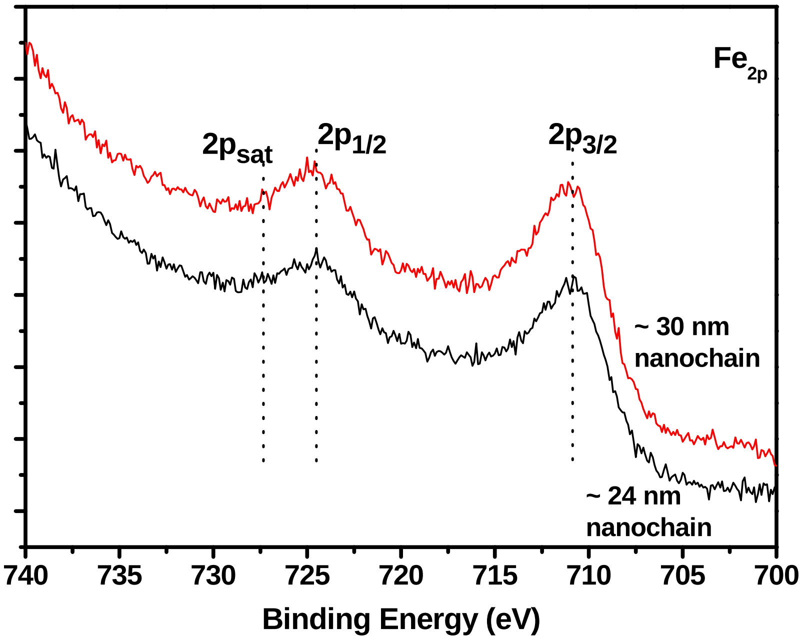

Fig. S3 XPS Fe2p spectra of ~24 nm diameter γ-Fe_2O_3 nanostructures stabilized by PP-MA (M_n≈2500) and ~30 nm diameter γ-Fe_2O_3 nanostructures stabilized by PP-MA (M_n≈8000). For both of the two nanochains, the two intensive peaks at Fe $2p_{3/2}$ (710.7 eV) and Fe $2p_{1/2}$ (724.3 eV) with only one satellite peak around Fe $2p_{1/2}$ shows good agreement with the reported spectra of γ-Fe_2O_3.[2]

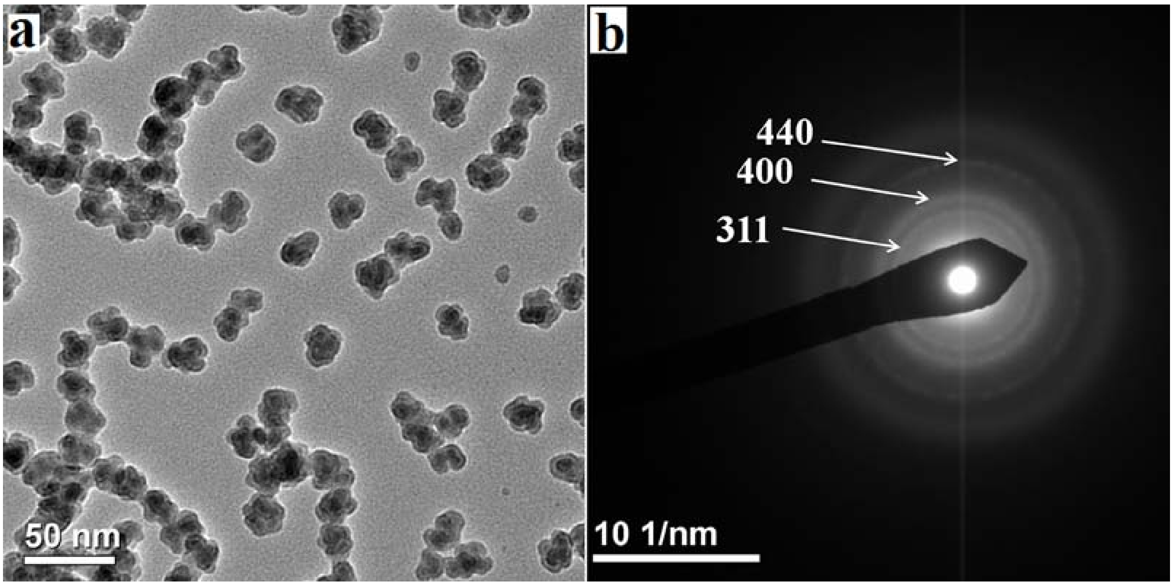

Fig. S4 a). TEM image and b). SAED patterns of γ-Fe_2O_3 nanostructures stabilized by PP-MA (M_n≈8000). The strong ring patterns are corresponding to (311), (400), and (440) planes of γ-Fe_2O_3 (PDF#39-1346). Reaction composition: 3.5 g $Fe(CO)_5$ in 100 mL xylene with 0.50 g PP-MA(M_n≈8000).

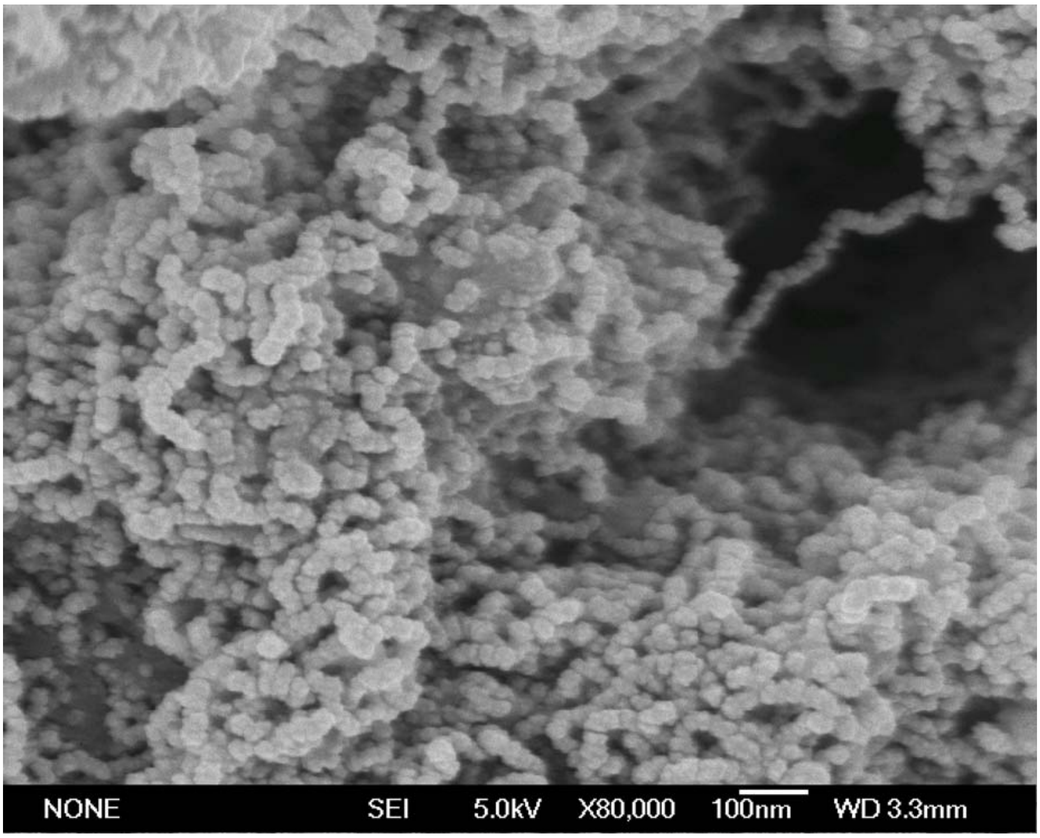

Fig. S5 SEM image of transition intermediate consists of γ-Fe_2O_3 nanostructures with partially nanoparticles and partially nanochains stabilized by PP-MA (M_n≈8000). Reaction composition: 3.5 g $Fe(CO)_5$ in 100 mL xylene with 0.50 g PP-MA (M_n≈8000).

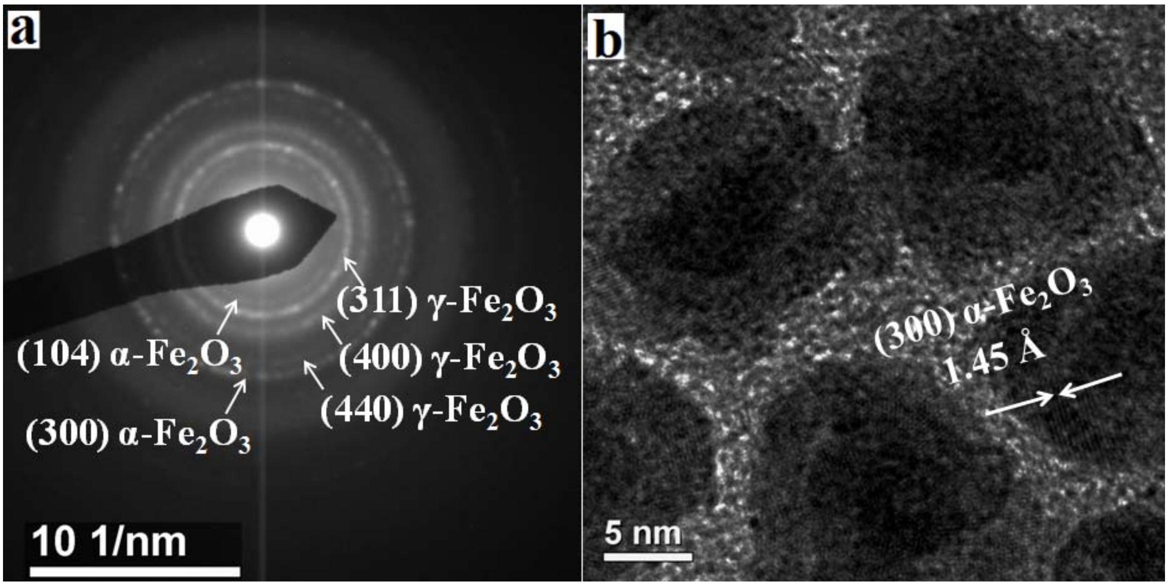

Fig. S6 a). SAED patterns, and b) HRTEM image of Figure 3b. In Fig. S5a, the strong ring patterns are corresponding to (311), (400), and (440) planes of γ- Fe_2O_3 (PDF#39-1346); and (104), (300) plane of α - Fe_2O_3(PDF#33-0664). In Fig. S5b, the 1.45 Å lattice spacing is indexed as the (300) plane of α - Fe_2O_3. Reaction composition: 3.5 g $Fe(CO)_5$ in 100 mL xylene with 0.50 g PP-MA (M_n≈2500).

When thermo-decomposing $Fe(CO)_5$ in xylene in the presence of surfactant PP-MA, oxidization took place during the nucleation and growth of small iron clusters. Therefore, the magnetic nanoparticles usually formed will be γ-Fe_2O_3. It is widely acknowledged that the bonding strength and bonding density on the surface of nanocrystal will control the growth of certain crystalline plane and further lead to different stacking sequence, which resulted in the formation of different crystalline phases.[3] Meanwhile, it has also been reported about the possession of maghemite (γ-Fe_2O_3)-like defects at the near surface regions of α- Fe_2O_3.[4] Therefore, α- Fe_2O_3 formed on the surface of γ-Fe_2O_3 in the presence of PP-MA is caused by the bonding density difference. With higher MA density of PP-MA (2500) than PP-MA (8000) at the same amount used (0.50 g in 100 ml xylene), crystalline lattice disorder would take place when denser bonding of PP-MA (2500) on the surface of these magnetic nanoparticles, therefore, the re-organization of γ-Fe_2O_3 is probably the reason to form α- Fe_2O_3 on its surface. Through the room temperature magnetic hysteresis measurement, the significantly decreased saturation magnetization (from 30.0 emu/g of flower shaped γ-Fe_2O_3 nanoparticles to 9.3 emu/g for the core-shell nanoprticles, see Figure S6) is another evidence that the existence of anti-ferromagnetic α- phase Fe_2O_3.

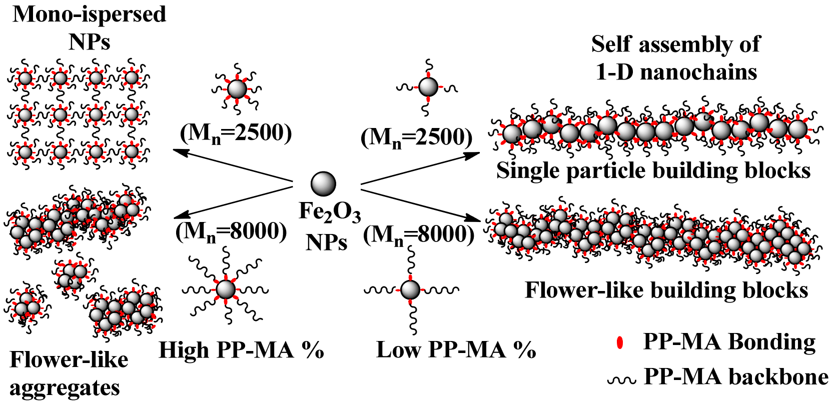

Scheme S4. The mechanism of different self-assembly morphologies.

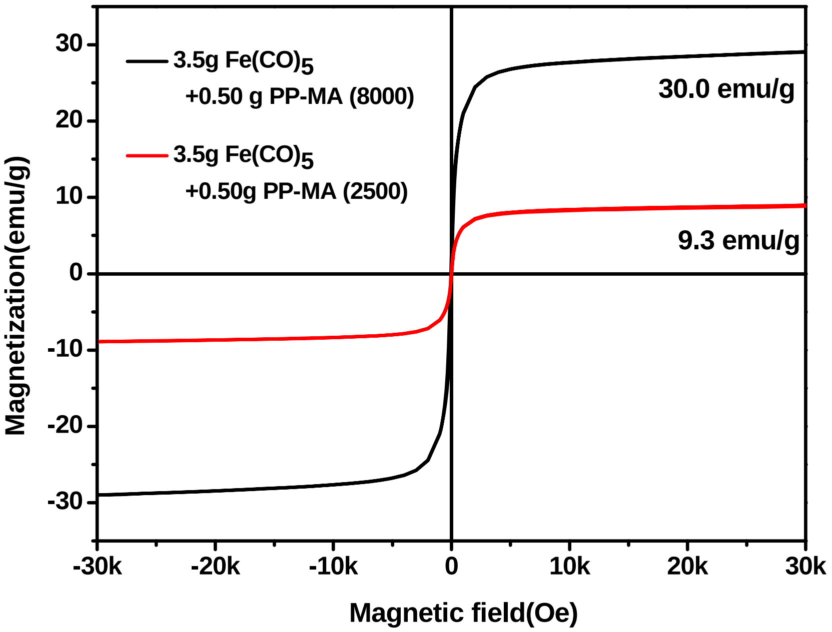

Fig. S7 Room temperature magnetic hysteresis loops of the γ- Fe_2O_3 flower shape nanostructures (with partially nanoparticles and partially nanochains, black curve) and γ- Fe_2O_3 - α-Fe_2O_3 core-shell nanoparticles (red curve) stabilized by PP-MA with different molecular weights (M_n≈2500 for red curve, and M_n≈8000 for black curve). (Reaction composition: 3.5 g $Fe(CO)_5$ in 100 mL xylene with 0.50 g PP-MA.

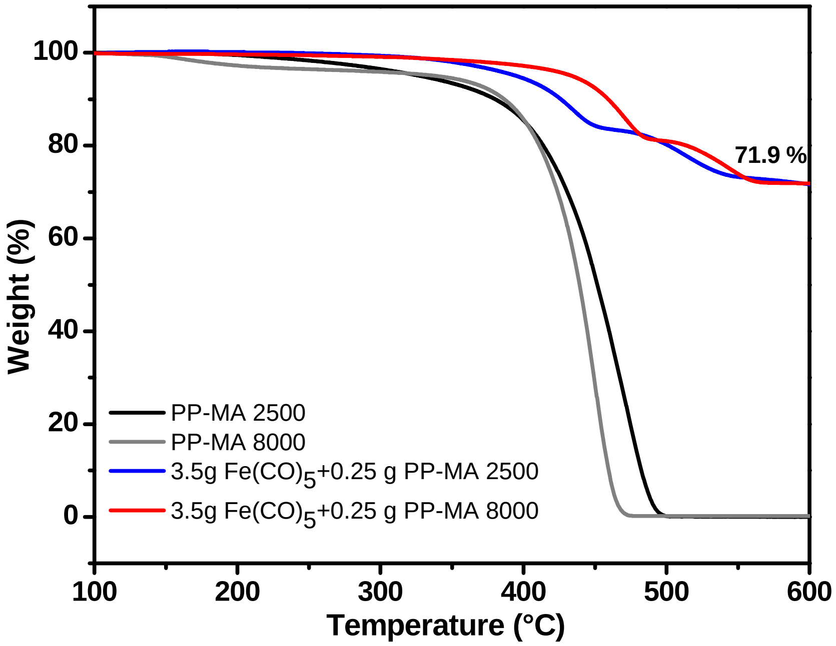

Fig. S8 TGA curves of the γ-Fe_2O_3 nanochains stabilized by PP-MA with different molecular weight. Reaction composition: 3.5 g $Fe(CO)_5$ in 100 mL xylene with 0.50 g PP-MA (Mn≈2500, 8000)

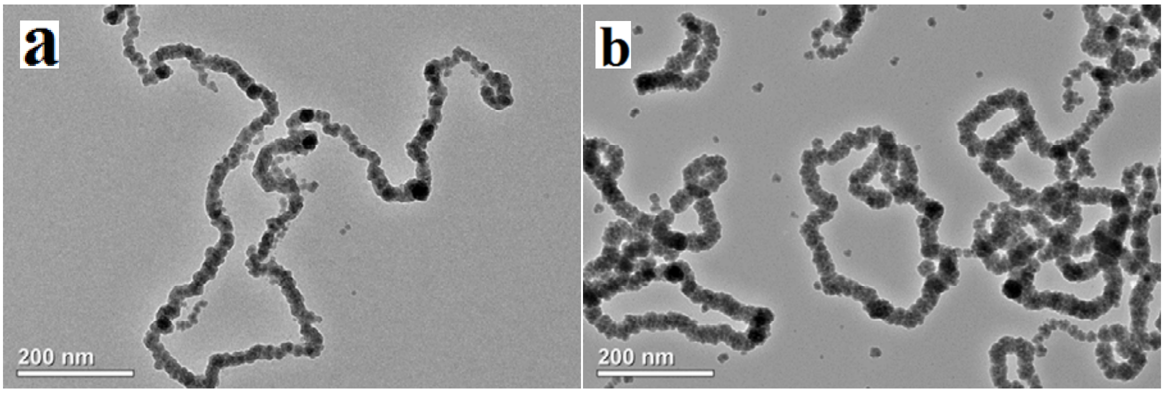

Fig. S9 TEM image of γ-Fe_2O_3 nanochains stabilized by PP-MA with M_n of (a) 2500, and (b) 8000 g/mol. Reaction composition: 3.5 g $Fe(CO)_5$ in 100mL xylene with 0.25 g PP-MA.

TGA curve (Fig. S8) demonstrates a 71.9 wt% particle loading for both high and low molecular weight PP-MA/nanochain γ-Fe_2O_3 nanocomposites. The saturation magnetization (M_s) of nanochain γ-Fe_2O_3 nanocomposites is 51.5 and 46.9 emu/g for PP-MA (M_n≈8000) and PP-MA (M_n≈2500) samples, respectively. The bulk γ-Fe_2O_3 is about 60-80 emu/g. It can be deduced that M_s of 51.5 and 46.9 emu/g can be converted to 71.6 and 65.2 emu/g for pure γ-Fe_2O_3 nanochains. This further confirms that these Fe_2O_3 nanochains are in γ-phase. The different weight loss onset temperature for the different nanochains is probably caused by the different configurations. As for the flower-shaped nanochains with larger diameter (~30 nm), every small nanoclusters were bound with PP-MA (8000), which resulted in relatively more PP-MA (8000) left among the flower-shaped clusters than the PP-MA (2500) since the smaller diameter nanochains have less surface area shielded among the single spherical nanparticle building blocks. In our previous work, we found the magnetic nanoparticles chain structure in polymer matrix can effectively block the heat transfer when the composites were exposed under heat radiation.[5] This is why the PP-MA (8000)/nanochain (~30 nm) composites have higher onset temperature compared with that of the counterpart with smaller diameter chain formed in PP-MA (2500). This is also auxiliary evidence that the magnetic γ-Fe2O3 nanochains was bound with PP-MA through the MA function groups. The lower M_s of smaller diameter (~24.0 nm) nanochains is probably caused by a magnetically disordered surface layer,[6] and the surface canting.[7] In addition, due to the higher M_s for 30.0 nm diameter 1-D γ-Fe_2O_3 nanochains, strong magnetic dipole-dipole attractions resulted in the formation of a closed loop, Fig. S9b, in order to minimize the magnetostatic energy;[8] which was not observed in the 24.0 nm diameter 1-D γ-Fe_2O_3 nanochains, Fig. S9a. For the coercivity difference, the reduction in size and dimension of the 1-D chain-like γ-Fe_2O_3 nanostructures may result in the variation of the magnetization reversal mechanism (which refers to the process that leads to a 180° re-orientation of the magnetization vector with respect to its initial direction, from one stable orientation to the opposite one), and thus leaded to an enhanced coercivity.[9, 10] Meanwhile, it is believed that the coercivity is especially depended on the shape anisotropy of the samples.[11-13]

Reference

1. Q. He, T. Yuan, S. Wei, N. Haldolaarachchige, Z. Luo, D. P. Young, A. Khasanov and Z. Guo, *Angewandte Chemie International Edition*, 2012, **51**, 8842-8845.
2. I. T. Kim, G. A. Nunnery, K. Jacob, J. Schwartz, X. Liu and R. Tannenbaum, *The Journal of Physical Chemistry C*, 2010, **114**, 6944-6951.
3. D. P. Dinega and M. G. Bawendi, *Angewandte Chemie International Edition*, 1999, **38**, 1788-1791.
4. I. Chernyshova, M. Hochella Jr and A. Madden, *Physical Chemistry Chemical Physics*, 2007, **9**, 1736-1750.
5. Q. He, T. Yuan, X. Zhang, Z. Luo, N. Haldolaarachchige, L. Sun, D. P. Young, S. Wei and Z. Guo, *Macromolecules*, 2013, **46**, 2357-2368
6. A. Millan, A. Urtizberea, N. Silva, F. Palacio, V. Amaral, E. Snoeck and V. Serin, *Journal of magnetism and magnetic materials*, 2007, **312**, L5-L9.
7. M. Morales, S. Veintemillas-Verdaguer, M. Montero, C. Serna, A. Roig, L. Casas, B. Martinez and F. Sandiumenge, *Chemistry of materials*, 1999, **11**, 3058-3064.
8. V. F. Puntes, K. M. Krishnan and A. P. Alivisatos, *Science*, 2001, **291**, 2115-2117.
9. C.-M. Liu, L. Guo, R.-M. Wang, Y. Deng, H.-B. Xu and S. Yang, *Chemical Communications*, 2004, **0**, 2726-2727.

10. B. Y. Geng, J. Z. Ma, X. W. Liu, Q. B. Du, M. G. Kong and L. D. Zhang, *Applied physics letters*, 2007, **90**, 043120-N.PAG.
11. Y. Leng, Y. Li, X. Li and S. Takahashi, *The Journal of Physical Chemistry C*, 2007, **111**, 6630-6633.
12. W. Zhou, L. He, R. Cheng, L. Guo, C. Chen and J. Wang, *The Journal of Physical Chemistry C*, 2009, **113**, 17355-17358.
13. Z. An, S. Pan and J. Zhang, *The Journal of Physical Chemistry C*, 2009, **113**, 1346-1351.